Biomass Conversion and Biorefinery (2025) 15:10773–10790
https://doi.org/10.1007/s13399-024-05821-w

ORIGINAL ARTICLE

Parthenium hysterophorus-derived iron-coated biochar: a sustainable solution for nitrate and phosphate removal from water

Izaz ul islam[1] · Mushtaq Ahmad[1,2] · Behzad Shah[2] · Hafiz Muhammad Ahmad[2] · Sara Janiad[3] · Nasrullah Shah[1] · Erdal Yabalak[4,5]

Received: 3 April 2024 / Revised: 24 May 2024 / Accepted: 3 June 2024 / Published online: 20 June 2024
© The Author(s) 2024

Abstract

Water bodies face severe pollution from industrial operations and other human activities, endangering biotic life worldwide. Nitrate and phosphate contamination poses a significant challenge globally. This study focuses on developing an efficient adsorbent, derived from *Parthenium hysterophorus* (*P. hysterophorus*), for nitrate and phosphate removal from water. Biochar, termed *P. hysterophorus* stem biochar (SBC), was prepared at 650℃ and further coated with iron, creating iron-coated stem biochar (ICSBC), to enhance adsorption potential. SEM, TEM, EDX, and FTIR analyses characterized raw and coated biochars. Comparative adsorption studies revealed that *P. hysterophorus* ICSBC exhibited high adsorption capacity (nitrate = N = 77.17 mg/g, phosphate = P = 83.93 mg/g) and removal efficiency (nitrate = 88.19%, phosphate = 95.89%). Batch experiments explored the effects of contact time, adsorbent loading, pH, and initial concentration. Kinetic and equilibrium models demonstrated that the pseudo-second-order kinetic and Langmuir isotherm models best fit the data (R^2 values: N = 0.9644, P = 0.98122, N = 93.68, P = 92.97, respectively). ICSBC's favorable attributes, including strong adsorption, low cost, and eco-friendliness, position it as an ideal adsorbent for nitrate and phosphate removal from contaminated water.

Keywords Pyrolysis · Nitrate · Phosphate · Adsorption · *Parthenium hysterophorus* · Iron-coated stem biochar

1 Introduction

Freshwater bodies receive substantial amounts of plant nutrients, such as nitrate and phosphate, each year due to various geochemical processes and human activities [1]. The excessive influx of nutrients into water bodies leads to eutrophication. The buildup of nutrients causes rapid growth of aquatic plants and algae, resulting in a depletion of dissolved oxygen. Eutrophication (excessive plants and algal growth) is a common issue among water bodies that contain a high concentration of nutrients, especially phosphates and nitrates, as they are essential for plants and algal growth. Eutrophication directly affects aquatic life by lowering dissolved oxygen

Izaz ul islam and Mushtaq Ahmad contributed equally to this work.

Highlights
- *Parthenium hysterophorus* biochar was utilized as a practical and effective biosorbent.
- Impregnating biochar with $FeCl_3$ and $FeSO_4$ enhances its ability to adsorb nitrate and phosphate.
- Iron-coated *P. hysterophorus* stem biochar (ICSBC) effectively removes nitrate and phosphate.
- A cost-effective, eco-friendly, and appealing choice for wastewater treatment was proposed.
- ICSBC exhibited high adsorption capacity of nitrate and phosphate.

✉ Nasrullah Shah
nasrullah@awkum.edu.pk

✉ Erdal Yabalak
yabalakerdal@gmail.com

[1] Department of Chemistry, Abdul Wali Khan University Mardan, Mardan 23200, Pakistan

[2] Tianjin Key Laboratory of Molecular Optoelectronic Science, Department of Chemistry, School of Science, Tianjin University, Tianjin 300072, China

[3] Department of Microbiology and Molecular Genetics, The Women University Multan, Multan, Pakistan

[4] Department of Chemistry and Chemical Processing Technologies, Technical Science Vocational School, Mersin University, Mersin 33343, Turkey

[5] Department of Nanotechnology and Advanced Materials, Mersin University, Mersin, Turkey

levels and can indirectly affect non-aquatic life by disturbing the food chain [2–4]. According to the WHO, the acceptable limits of phosphate and nitrate in surface and wastewater are 0.5 mg/L and 40 mg/L, respectively [5]. In drinkable water, the presence of nitrate ions in excess is a potential public health hazard and is responsible for methemoglobinemia in infants, i.e., blue baby syndrome. According to the Environmental Protection Agency (EPA, 1990), chronic nitrate exposure can cause diseases like spleen hemorrhage, diuresis, and enhancement in the starch deposits. The toxicity of phosphate in humans includes rhabdomyolysis, tumor lysis syndrome, and renal function impairment [6]. To protect aquatic and terrestrial life from the adverse effects of phosphate and nitrate pollution, its removal from wastewater before it discharges to water bodies is mandatory.

Various biological and physicochemical processes have been used to treat wastewater and water enriched with dissolved nutrients. The mechanism of biological processes is based on the transformation of phosphate and nitrate anions from the liquid phase into the sludge phase. The biological process hardly shows a removal efficiency of 30%. Hence, biological process all alone is not sufficient for the treatment of wastewater enriched with phosphate and nitrate [7–9]. Physicochemical processes like chemical precipitation, membrane filtration, and ion exchange have been reported previously, but they also have drawbacks. Chemical precipitation is faced with the challenge of excessive influx of a significant amount of chemicals and issues of waste disposal. Membrane processes, degradation of the membrane, scaling, high cost of maintenance, and fouling are the factors that limit the use of membrane filtration for the treatment of contaminated water at the bulk level [10]. Similarly, besides their high costs and lengthy operational processes, all other techniques have many drawbacks that limit their use for removing nitrate and phosphate anions from water, especially at the bulk level. Therefore, there is an urgent requirement to develop a removal technique that demonstrates high efficiency, affordability, minimal or no waste disposal concerns, and environmental friendliness. Among the various removal techniques, adsorption is considered the most reliable method for eliminating nitrate and phosphate from wastewater at the bulk level because of its minimum costs, highly efficient, fast, and environmentally friendly nature.

A wide range of adsorbents, such as carbon, graphene, and silica-based adsorbents, are employed in the adsorption technique. However, like many removal methods, these adsorbents tend to be costly and less effective and often produce additional waste. Hence, the researchers focus on developing such adsorbents for the process of adsorption that do not possess all the above drawbacks.

Biochar is a carbonaceous, highly porous, charcoal-like material prepared in an oxygen-deficient environment from 450 to 900 °C. Compared to other adsorbents, biochar possesses properties like high adsorption capacity, maximum efficiency, and cheapness, making it the most suitable adsorbent for adsorption technique. Various biomasses, like peanut shells, corn straw, rice straw, and corn cob, can be used for biochar preparation [1]. Several procedures have previously been employed to modify biochar, including chemical reduction, chemical oxidation, and metal impregnation, to enhance the biochar adsorptive potential. Among them, metal impregnation is considered the most effective mode of biochar modification. During this process, metal in the form of nanoparticles is coated onto biochar, enhancing its adsorption capacity and removal efficiency by improving its surface chemistry [11]. The commonly used metals are iron, silver, zinc, and magnesium [11] for metal impregnation. Among these metals, the impregnation with iron is encouraging due to its magnetic properties, the maximum capability of adsorption, and the highly effectual capability of solid-liquid separation.

The spread of *P. hysterophorus* over Asia and its native region, South and Central America, is serious as it aggressively competes and affects the growth of other beneficial flora [12, 13]. *P. hysterophorus* is a non-economic weed, so the development of adsorbent from it is the possible solution to the problem of its effects on agro-habitats and the high cost of conventional adsorbents. Numerous investigations revealed that *P. hysterophorus* burning produces severe environmental problems that badly affect human health. The *P. hysterophorus* constituent affirmed that it has good potential to be used to develop efficient adsorbents for removing nitrate and phosphate ions from polluted water [13].

Therefore, the basic aim of this study is to use *P. hysterophorus* as a raw material for the preparation of biochar and then impregnate it with $FeCl_3{\cdot}7H_2O$ and $FeSO_4{\cdot}7H_2O$ to boost its efficiency. The prepared modified and unmodified biochars were examined by FTIR, EDX, SEM, TEM, and XRD for functional group, elemental, and morphological analysis. Batch sorption experiments were conducted to investigate nitrate and phosphate adsorption behavior onto the biochar surface at various pH, adsorption time, dosage of ICPBC, and preliminary concentration of the adsorbate. Kinetics and isotherm models were used to study nitrate and phosphate adsorption onto ICPBC which were also investigated. The main theme of this study is to prepare a useful adsorbent using *P. hysterophorus*, impregnate it with iron, and investigate the nitrate and phosphate adsorption from wastewater.

2 Experimental

2.1 Materials

In this study, analytical-grade chemicals and reagents were used. Potassium nitrate and potassium phosphate were purchased from BDH. NaOH, HCl, ferrous sulfate

heptahydrate ($FeSO_4 \cdot 7H_2O$), and ferric chloride hexahydrate ($FeCl_3 \cdot 6H_2O$) were purchased from Merck. Double-distilled water was used for solution preparation and cleansing of glassware. *P. hysterophorus* stems and roots were used as raw materials for the preparation of biochar.

2.2 Methods

2.2.1 Preparation of biochar

Biochar preparation involved gathering *P. hysterophorus* weed from Mardan, Khyber Pakhtunkhwa, Pakistan. The weed samples were sliced into smaller pieces using a cutter. To detach the dust and tacky mud, the sample was washed several times with tap water followed by double-distilled water. The samples were dried at 85 °C using a hot air oven for 36 h. As the samples have dried, a portion from it enclosed in the platinum foil was shifted to the furnace chamber. The furnace chamber is designed to provide an oxygen-deficient environment for the pyrolysis of the sample. At a heating rate of 15 °C/min, the furnace temperature was increased to 650 °C, and keep the furnace temperature at this value for 1 h. After the residence time of 1 h, the sample was shifted from the furnace chamber to the desiccator and kept there until the sample cooled up in the absence of air. The corresponding biochar obtained from the pyrolysis was crushed and sieved to obtain particles of uniform diameter. The sample obtained from all the above procedures was named *P. hysterophorus* stem biochar (SBC) and *P. hysterophorus* root biochar (RBC).

2.2.2 Coating (modification) of *P. hysterophorus* biochar (SBC and RBC) with iron

To coat the *P-Stem* and *P-Root* biochar (SBC and RBC) with iron, we first prepared a solution by dissolving 7 g of $FeCl_3 \cdot 6H_2O$ and 7 g $FeSO_4 \cdot 7H_2O$ in 80 mL of water in a beaker, as reported in our previous work [31, 14] . Likewise, a suspension of SBC and RBC was prepared by adding 8–10 g of each sample to separate beakers containing 500 mL of double-distilled water. These solutions and suspension were mixed and placed on a magnetic stirrer. The mixture was stirred at 120 rpm for 1.5 h using the magnetic stirrer. After this duration, we adjusted the pH of the solution by adding HCl and NaOH until the final pH reached 7, therefore facilitating the chemical co-precipitation of iron over the *P. hysterophorus* biochar. The solution was then filtered using filter paper, allowing the liquid to pass through the paper while biochar residue on the paper. This biochar residue was subsequently dried in a hot air oven at 60 °C for 24 h. Upon completion of the drying process, they were labeled as iron-coated *P. hysterophorus* stem biochar (ICSBC) and *P. hysterophorus* iron-coated root biochar (ICRBC) [14].

2.3 Characterization

Functional group analysis, elemental composition, and morphological characteristics of SBC and ICSBC were investigated using FTIR, EDX, SEM, and TEM. Via energy-dispersive X-ray spectroscopy (EDX) U.K, JSM5910, INCA200/Oxford instruments), scanning electron microscope (SEM. JSM5910 Model JEOL, Japan), and transmission electron microscope (JEM-2100, manufactured by JEOL Japan), the elemental composition and surface morphology were investigated. The functional groups were analyzed using Fourier-Transform Infrared Spectroscopy (FTIR-650, Tianjin Gangdong Sci. & Tech. Co., Ltd.).

2.4 Batch adsorption experiment

The nitrate and phosphate 1000 mg/L of stock solution were prepared by dissolving 0.63064 g of KNO_3 and 1.723 g of KH_2PO_4 in 1000 mL of double-distilled water. The standard solution was diluted to 10, 15, 20, 25, 30, 35, 40, 45, 50, 55, 60, 65, and 70 mg/L using dilution factor. Utilizing a 100 mL Erlenmeyer flask, all the batch adsorption experiments were carried out. Magnetic stirrers were used to agitate the flasks containing 50 mL of nitrate and phosphate at a speed of 120 rpm at a temperature of 25 ± 2 °C. To investigate the effect of ICSBC dosage (0.02, 0.03, 0.04, 0.05, 0.06), time of contact (5, 10, 20, 50, 120, 180, 240, 300, 360, 420), pH of the solution (2, 3, 4, 5, 6, 8, 10, 12), and adsorbate initial concentration (10, 15, 20, 25, 30, 35, 40, 45, 50, 55, 60, 65, and 70 mg/L) on the adsorption capability of nitrate and phosphate, the batch adsorption experiments were carried out. The initial pH of the solution was regulated using 0.1 M NaOH and 0.1 M HCl solutions. Using filter paper, the mixture obtained after the completion of the adsorption process was filtered. A UV-visible spectrometer revealed the nitrate and phosphate total concentration in the suspended solution. The removal efficiency and the adsorption capacity of ICSBC and ICRBC for nitrate and phosphate at time t [$q_{t,}$ mg/g] and equilibrium [$q_{e,}$ mg/g] are determined using Eqs. (1), (2), and (3), respectively.

$$\% \text{ Removal} = \frac{(C_o - C_e)}{C_0} \times 100 \quad (1)$$

$$Q_t = \frac{(C_o - C_t)}{M} \times V \quad (2)$$

$$Q_e = \frac{(C_o - C_e)}{M} \times V \tag{3}$$

C_t, C_e, and C_o imply the nitrate and phosphate solution concentration in mg/L at any time t, at commencement time, and equilibrium, M represents the biochar mass added (g), and V is the solution volume in L of the test sample.

2.5 Point of zero charge

The surface alkalinity and acidity of the prepared biochar were characterized using pH_{pzc}. Using the pH shift method, the pH-dependent pH_{pzc} was determined. In separate Erlenmeyer flasks, 40 mL of 0.1 M NaCl solutions was taken, and using 0.1 M HNO_3 and 0.1 M NaOH solutions, the pH was adjusted according to our desired range in step size of one. A particular amount of ICSBC was added to the NaCl solution and subjected to stirring for 48 h. The final pH was measured, and the differential ΔpH was investigated by subtracting the pH_f from pH_i. This ΔpH was then plotted against pH_i, and the corresponding pH_{pzc} was calculated.

2.6 Adsorption kinetics

Kinetic models are used to investigate the rate at which adsorbate adsorbed onto the adsorbent during the process of adsorption. To study the adsorption of nitrate and phosphate onto the ICSBC, two models, namely, the pseudo-first-order kinetic model and pseudo-second-order kinetic model, were used. The linear form of these models is represented by Eqs. (4) and (5) [15].

$$\ln\left(q_e - q_t\right) = \ln q_e - K_1 t \tag{4}$$

$$\frac{t}{q_t} = \frac{1}{K_2 q_e^2} + \frac{1}{q_e} t \tag{5}$$

2.7 Adsorption isotherms

In aqueous media, adsorption isotherms were used to describe the relationship between the adsorption capacity and concentration at equilibrium. Adsorption isotherms play a vital role in understanding the physiochemical essence and calculation of the adsorption capacity. Three isotherms' models, namely, Freundlich, Langmuir, and Sips models, were employed to find out the good-fit model of the adsorption process. The linear form of the Freundlich, Langmuir, and Sips isotherm model is represented by Eqs. (6), (7), and (8), respectively [15].

$$\log q_e = \log K_f + \frac{1}{n} \log C_e \tag{6}$$

In Eq. (6), $1/n$ and K_f are adsorption intensity and Freundlich constant relating to adsorption capacity, respectively, while C_e and q_e are the equilibrium concentration and adsorption capacity.

$$\frac{1}{q_e} = \frac{1}{K_L q_{\max} C_e} + \frac{1}{q_{\max}} \tag{7}$$

In Eq. (7), K_L is the Langmuir constant, and $q_{\max}$ is the maximum possible adsorption capacity of adsorbent for adsorbate.

$$q_e = \frac{q_m \left(bC_e\right)^{\frac{1}{n}}}{1 + \left(bC_e\right)^{\frac{1}{n}}} \tag{8}$$

In Eq. (8), n is a fitting parameter, b is an equilibrium constant, and q_m is the maximum adsorption capacity.

2.8 Desorption experiment

A specific amount of ICSBC was added to the desired nitrate and phosphate solution concentration. After the equilibrium time, this suspension was subjected to filtration; as a result, the adsorbent was separated from the filtrate. The filtrate was analyzed for the remaining concentration of nitrate and phosphate and the adsorption efficacy was measured. The adsorbent separated as a result of the filtration process was dried for 48 h at 55 °C in a hot air oven. This dried ICPSBC was mixed with 70 mL of 0.2 M NaOH and stirred using magnetic stirrers at 120 rpm. Finally, the adsorbent was separated via filtration, and the filtrate was determined for the desorbed amount of nitrate and phosphate [15, 16].

2.9 Analysis of data

All the experiments were examined in triplicate. Origin software (2021) was used for analyzing the experimental data.

3 Results and discussion

3.1 Selection of efficient adsorbent by removal efficiency and their potential of the adsorption

To achieve efficient removal of nitrate and phosphate from contaminated water, various adsorbents' removal efficiencies and adsorptive capabilities were analyzed under comparable conditions. The adsorbents used in this study were raw *P. hysterophorus* stem (SBC), root (RBC), iron-coated stem (ICSBC), and (ICRBC). Four 80-mL solutions of 40 mg/L of nitrate and phosphate concentration were chosen for the investigation. These four sample solutions were labeled

according to the type of adsorbent added. The sample to which *P. hysterophorus* stem biochar was added is labeled as SBC, to which iron-coated stem biochar was added is labeled as ICSBC, and sample solution to which *P. hysterophorus* root and iron-coated root biochar was added is labeled as RBC and ICRBC. 0.06 g of the respective adsorbent was added to these samples using magnetic stirrers; these samples were agitated at a speed of 120 rpm for 180 min, and the pH of the solutions was maintained between 2 and 3. After the process of adsorption, the sample solution was analyzed for the remaining concentration of nitrate and phosphate using a UV-visible spectrometer. The results obtained are summarized in Fig. 1.

From Fig. 1, we can conclude that for the effective removal of nitrate and phosphate from polluted water, *P. hysterophorus* iron-coated stem biochar (ICSBC) is an efficient adsorbent with a maximum removal efficacy of 88.19% for nitrate and 95.89% for phosphate. Similarly, the maximum adsorption capacity for nitrate and phosphate is 77.17 mg/g and 83.91 mg/g. Thus, among all four adsorbents prepared from the *P. hysterophorus* weed, iron-coated stem biochar (ICSBC) is selected for the rest of the studies due to its maximum effectiveness.

3.2 Characterization of SBC and ICSBC

Different methods were used to characterize biochar, and the findings are summarized below.

SBC and ICSBC EDX spectra are shown in Fig. 2A, B. Figure 2A reveals that carbon (58.08%), oxygen (21.78%), and silicon (10.48%) constitute the basic elemental composition of raw biochar by weight. The fundamental elemental composition of impregnated biochar is carbon (29.23%), oxygen (38%), silicon (13%), and iron (18.80%). When we compared the EDX spectra of both raw and impregnated

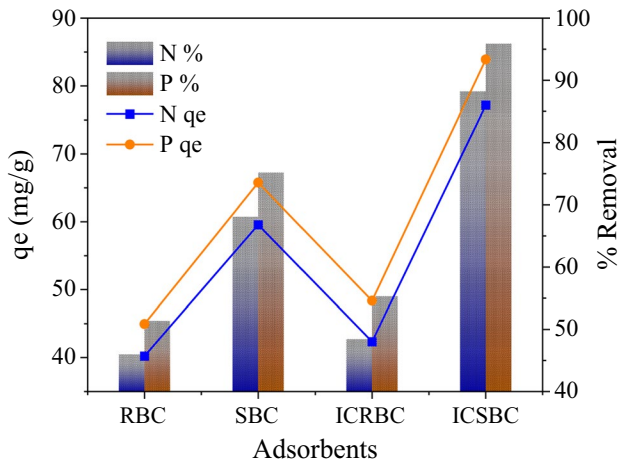

Fig. 1 Comparative analysis of different adsorbents for nitrate and phosphate removal from wastewater

biochar, we can conclude that there is a minimal amount of iron (0.09%) present in the spectrum of raw biochar, which may be attributed to the memory effect, while a considerable amount of iron is present (18.03%) in impregnated biochar. From this, we can conclude that iron in the form of iron oxide (Fe_2O_3) is successfully adsorbed onto the surface of raw stem biochar.

The SEM along with elemental mapping and TEM micrographs of SBC and ICSBC are shown in Figs. 3 and 4. The surface morphological analysis of the SBC and ICSBC shows that the ICSBC surface is rougher and more porous than the SBC's morphology. This heterogeneous surface morphology of the ICSBC is associated with the impregnation of the raw biochar with iron that grasps the micropores and results in macropores that enhance the adsorption of nitrate and phosphate from contaminated water. The presence of small particles on the surface of ICSBC is the particles of iron oxide that are formed due to chemical co-precipitation. The micrographs of TEM revealed that the surface of ICSBC is covered with crystals compared to SBC, as shown in Fig. 4. The presence of these crystals supports that iron oxides and hydroxides are successfully deposited onto the surface of ICSBC and the coating of SBC with iron is successfully achieved. Figure 3B, D shows the elemental mapping of SBC and ICSBC. From elemental mapping, it can be seen that oxygen, carbon, silicon, and calcium are widely distributed throughout the surface of SBC, while oxygen, carbon, silicon, and iron are the main elements present in the ICSBC.

The FTIR analysis (Fig. 5) identified many functional groups on the biochar surface. The peak at 873 and 580 cm^{-1} in the spectra of ICSBC refers to the presence of the Fe-O group stretching vibration [17]. In the spectra of SBC and ICSBC, the peaks that appeared at 1538 cm^{-1} and 1413 cm^{-1} denote the presence of the C-O-C and –COO groups [18]. The peaks at 1627 cm^{-1} of SBC point out the presence of ketonic and carbonyl group bond [19, 20]. The absorption peaks present at 2892 cm^{-1} of SBC and 2890 cm^{-1} ICSBC signify the stretching of the aliphatic group -(CH_n) [20]. The bands at 3442 cm^{-1} of SBC and 3440 cm^{-1} of ICSBC refer to the existence of –OH group stretching vibration [21]. In the FTIR spectra of P-ICSBC, the band present at 1085 cm^{-1} corresponds to the presence of P-O bond stretching vibration. Moreover, in the spectra of N-ICSBC, the peak at 1556 cm^{-1} corresponds to the N = O stretching vibration and NO_3 symmetric and asymmetric peaks are observed at 1384 cm^{-1} and 825 cm^{-1}. The spectra of SBC, ICSBC, P-ICSBC, and N-ICSBC exhibit differences, indicating modifications as a result of the coating process and after the adsorption process.

By comparative analysis of both the spectra, it can be seen that peak shifts occur from 3440, 2892, 1627, and 1538 cm^{-1} in the spectra of SBC to 3442, 2890, 1413, 873,

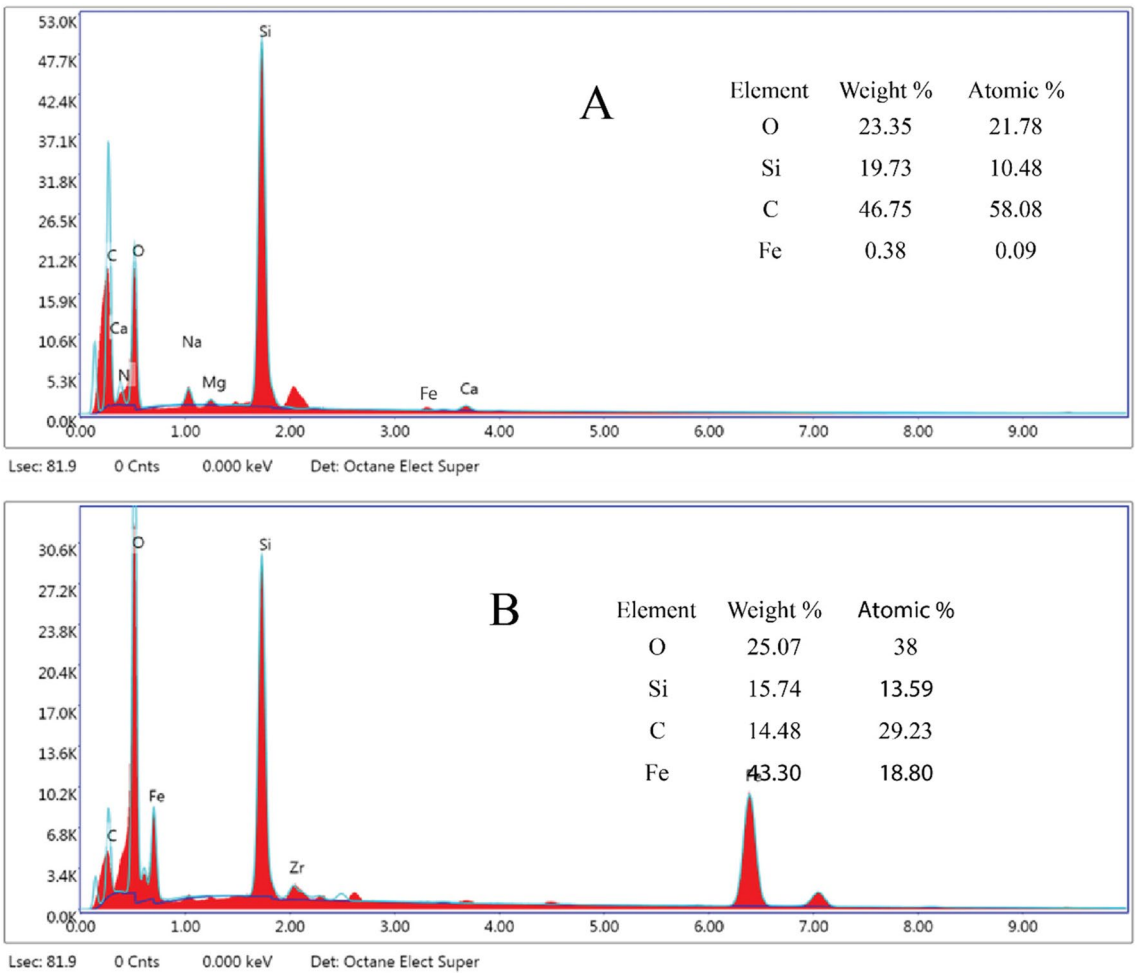

Fig. 2 EDS elemental analysis graphs for SBC (**A**) and ICSBC (**B**)

and 580 cm^{-1} in the spectra of ICSBC. This shift in the peaks value and change in the intensity of peaks confirm the successful coating of SBC.

XRD analysis was performed to check the crystallinity and coating of SBC and ICSBC. Figure 6 represents the XRD diffractograms of SBC and ICSBC. The diffractogram of SBC reveals that it is diffuse, which corresponds to the amorphous nature of our prepared SBC. In the diffractogram of ICSBC, a number of peaks appeared at 30.1°, 35.5°, 43.1°, 53.7°, and 57.3° that signify the successful coating and the presence of Fe_3O_4.

3.3 Effect of adsorbent dosage

The selection of proper adsorbent dosage is necessary to check the potential of adsorbent for adsorptive removal of pollutants from aqueous solution. To study the effect of adsorbent dosage on the removal efficiency and adsorption capacity of ICSBC for nitrate and phosphate, some adsorbent doses (0.02 to 0.06) were applied for adsorptive removal of nitrate and phosphate from aqueous solution while keeping all other parameters fixed [22], and the results are shown in Fig. 7. From Fig. 7, it can be seen that the removal efficiency of ICSBC for nitrate and phosphate increased from 54.57 to 97.15% and from 58.03 to 99.22%, respectively, with an increase in ICSBC dosage from 0.02 to 0.06 g, because, with the increase in adsorbent dosage, the number of active sites available for analyte adsorption also increases leading to efficient adsorption of adsorbate (nitrate and phosphate) which result in an increase in the removal efficiency of ICSBC for the analyte (nitrate and phosphate) [23]. In contrast, the adsorption capacity of ICSBC for the analyte (nitrate and phosphate) decreased from 95.4 to 56.6 mg/g and from 101.5 to 57.8 mg/g, respectively, with the increase in adsorbent dosage from 0.02 to 0.06 g.

The decrease in adsorption capacity with the increase in adsorbent dosage is due to the rise in the number of available active sites; the ratio of available active sites to analyte ions (nitrate and phosphate) also increases, which

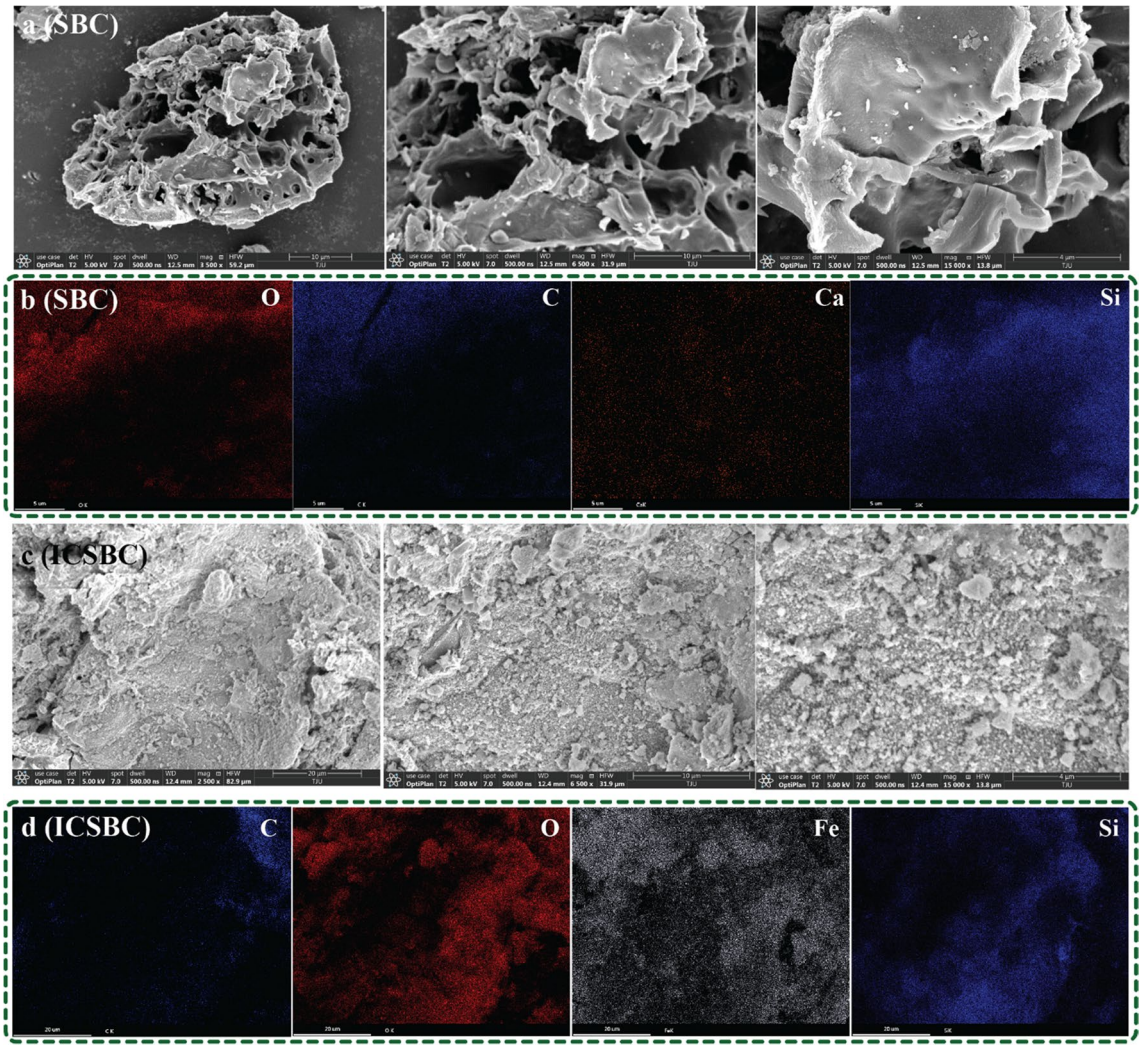

Fig. 3 SEM images of SBC and ICSBC and elemental mapping

results in unsaturated active sites leading to the lower adsorption capacity of ICSBC for nitrate and phosphate [24]. 0.04 g of ICSBC was found to be the optimum adsorbent dosage for 70 mL of 50 mg/L solutions of nitrate as well as of phosphate, because, at 0.04 g dosage, ICSBC shows simultaneous maximum adsorption capacity and removal efficiency for nitrate ($q_e = 77.17$ mg/g, %=88.19) as well as phosphate ($q_e = 83.91$ mg/g, %=95.89) [15]. Similar results were also obtained from previous studies [25].

3.4 Point of zero charge

Adsorbent point of zero charge (PZC) plays an active role in adsorbent surface chemistry, especially adsorbent surface charge. Several batch adsorption experiments were performed to measure PZC (pH_{PZC}) for ICSBC; the analysis results are shown in Fig. 8. As can be seen in Fig. 8, pH of 5 is found to be PZC for ICSBC, which means that at a pH lower than 5, the surface of ICSBC is positively charged, which would be electrostatically favorable for the adsorption of anions (nitrate and phosphate) leading to higher values of adsorption capacity and removal efficiency of ICSBC for anions (nitrate and phosphate) [24]. In the same way at pH higher than 5, the surface of ICSBC becomes negatively charged and electrostatically unfavorable for adsorption of anions (nitrate and phosphate) resulting in low adsorption capacity and removal efficiency of ICSBC for anions. For the study of the effect of pH on the adsorption of nitrate and phosphate on ICSBC, it was observed that the adsorption of nitrate and phosphate on ICSBC decreases with an increase in pH; this is because with the rise in pH, the surface of ICSBC becomes less positively charged, and as pH increases beyond five, it becomes negatively charged which electrostatically repels negatively charged nitrate and phosphate ions. So, with the

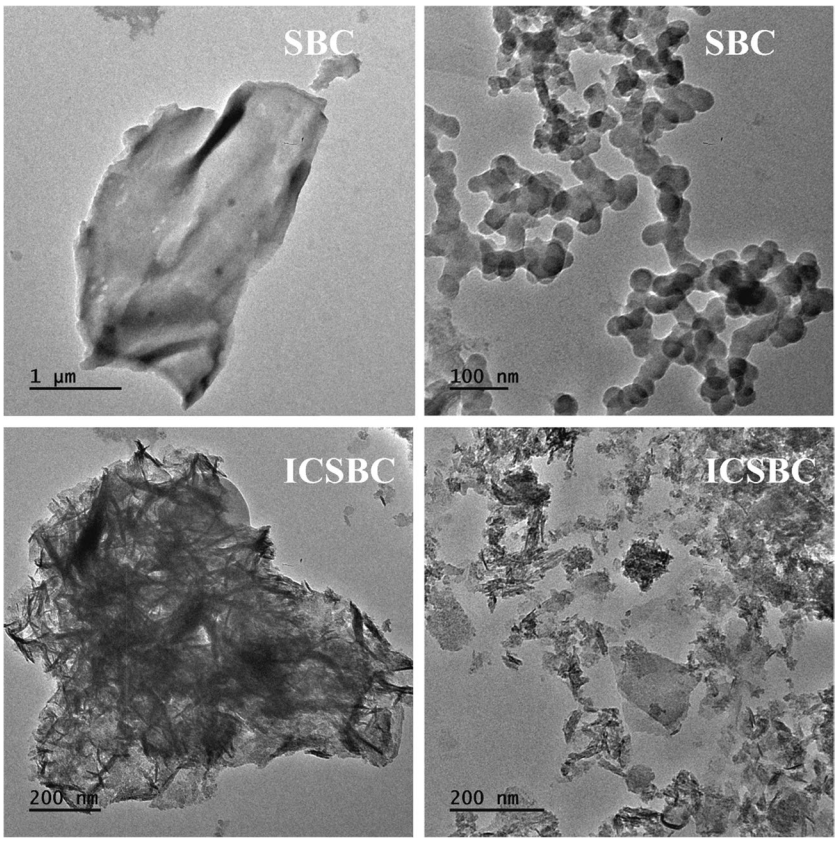

Fig. 4 TEM images of SBC and ICSBC

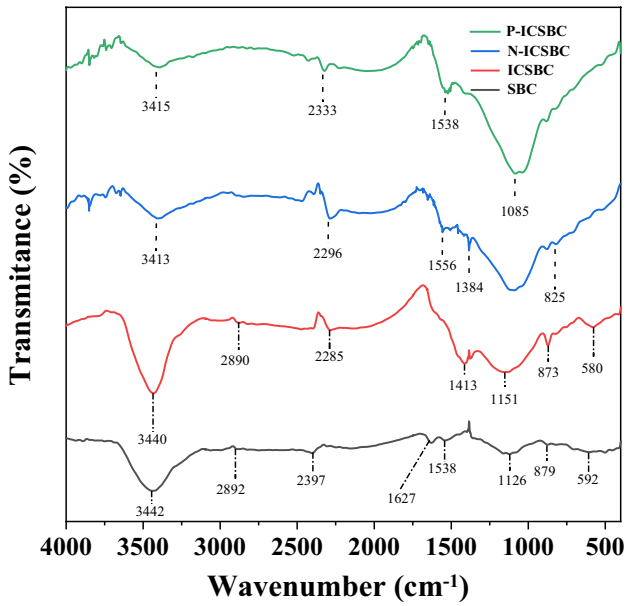

Fig. 5 FTIR spectra of SBC and ICSBC (before adsorption) and P-ICSBC and N-ICSBC (after adsorption)

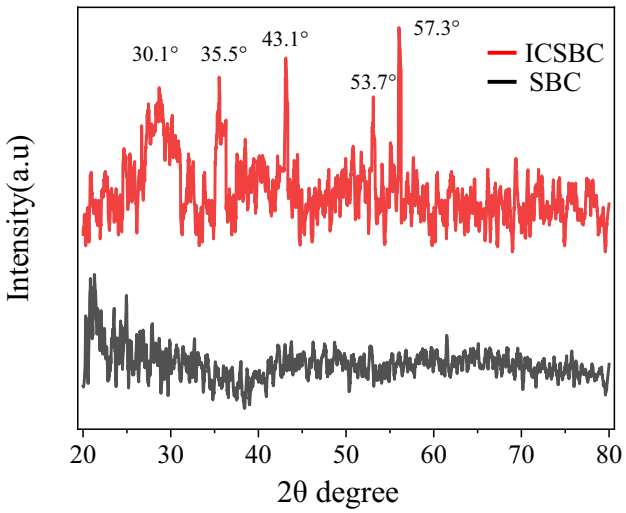

Fig. 6 XRD spectra of SBC and ICSBC

rise in pH, the electrostatic attractive interaction between adsorbate becomes an electrostatic repulsive interaction, which decreases the adsorption of anionic adsorbate with an increase in pH.

3.5 Effect of pH on the phosphate and nitrate adsorption capacity

The aqueous solution pH sensitively affects the adsorption of the analyte by the adsorbent, as pH affects the properties of both, the analyte and adsorbent. Several batch adsorption experiments were performed to investigate the effect

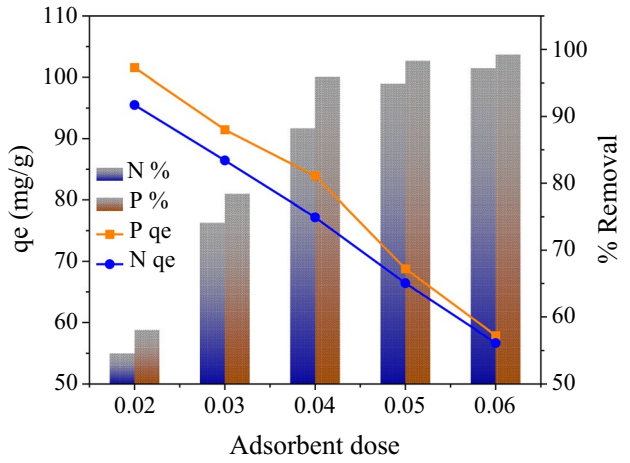

Fig. 7 The effect of adsorbent dosage on q_e and % removal of ICSBC for nitrate and phosphate

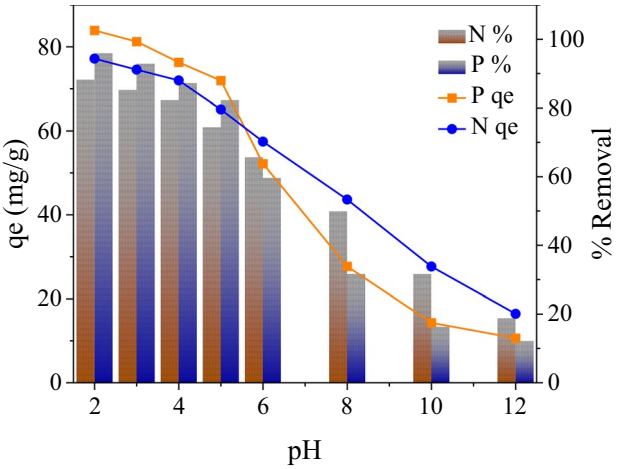

Fig. 9 Effect of pH on q_e and % removal of ICSBC for nitrate and phosphate

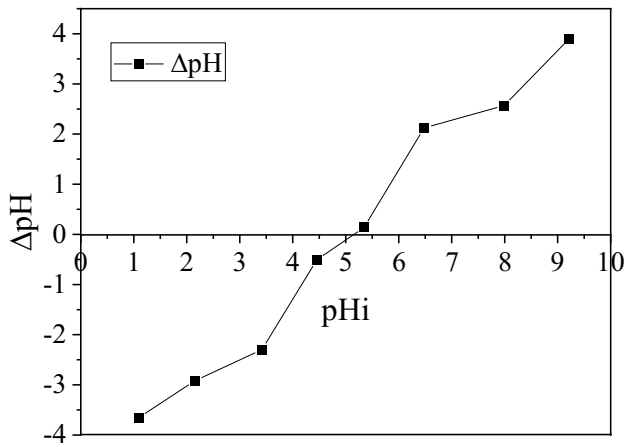

Fig. 8 Point of zero charge for ICSBC

of aqueous solution pH on the adsorption of phosphate and nitrate on the adsorbent. The results of the pH study are shown in Fig. 9. By measuring the final pH of the filtrate, it was observed that the final pH of the filtrate was higher for the initial pH lower than 6, while in contrast, the final pH of the filtrate was found lower for the initial pH higher than 6. This kind of behavior can be the result of the protonation and deprotonation of adsorbent surface hydroxyl groups. From the pH study, it was found that the removal efficiency and adsorption capacity of ICSBC for both phosphate and nitrate decrease with an increase in pH, and the highest adsorption capacity and removal efficiency for both nitrate (q_e = 77.1, % = 88.1) and phosphate (qe = 83.91, %= 95.89) were obtained at pH 2. The decrease in removal efficiency and adsorption capacity of ICSBC for nitrate and phosphate, with a change in pH, can be attributed to the shift in point of zero charge of ICSBC and to the change in the hydroxyl ion concentration, which actively competes with nitrate and phosphate for active sites present on ICSBC surface, with the shift in aqueous solution pH [22]. From the point of zero charge analysis, it was found that the PZC value for ICSBC is 5, which means at pH higher than 5 the surface of ICSBC is negatively charged, while at pH lower than 5 the ICSBC surface is positively charged. So, it can be concluded that at lower pH, the surface of ICSBC is positively charged and electrostatically attracts negatively charged nitrate and phosphate ions, resulting in high adsorption capacity and removal efficiency of ICSBC for nitrate and phosphate. With the increase in pH, the ICSBC surface tends to become less positively charged, and when pH crosses 5, the adsorbent becomes negatively charged and electrostatically repels nitrate and phosphate ions, resulting in lower adsorption capacity and removal efficiency of ICSBC for nitrate and phosphate.

Similarly, with the increase in the pH, the concentration of hydroxyl ions increases, which compete with negatively charged phosphate and nitrate ions for active sites on the ICSBC surface, which results in a decrease in removal efficiency and adsorption capacity of ICSBC for nitrate and phosphate with the increase in pH. From Fig. 9, it can be seen that the removal efficiency and adsorption capacity of ICSBC for nitrate fall uniformly with the increase in pH, but for phosphate, it falls abruptly with the rise in pH, significantly beyond five. This diverse behavior of ICSBC for nitrate and phosphate with the decrease in pH could be attributed to the change in speciation of nitrate and phosphate with the change in pH. The removal efficiency of ICSBC regularly falls for nitrate with the increase in pH because the speciation of nitrate is independent of pH and > 99% present in NO_3^-. The phosphate speciation is highly pH-dependent, and based on phosphate water chemistry,

phosphate has three pKa values of 2.2, 7.2, and 12.4. In pH 2.2 to 7.2, phosphate predominantly exists in the monovalent form of $H_2PO_4^-$, while at pH range from 7.2 to 12.4, it predominantly exists in the divalent form of HPO_4^{-2} [15, 26]. With the increase in pH, HPO_4^{-2} become the dominant form, which is difficult to be adsorbed on the ICSBC surface as compared to $H_2PO_4^-$; this is because the adsorption-free energy of HPO_4^{-2} is higher than $H_2PO_4^-$, which makes HPO_4^{-2} unfavorable for adsorption; this causes an abrupt decrease in removal efficiency and adsorption capacity of ICSBC for phosphate [23, 27]. In the end, it was concluded that nitrate and phosphate could be efficiently removed from wastewater by adsorption on ICSBC at a pH range from 2 to 5; similar results were also found by previous studies [15, 28].

3.6 Effect of initial concentration

The effect of initial adsorbate (nitrate and phosphate) concentration was investigated on the removal efficiency and adsorption capacity of ICSBC, and the results of the analysis are shown in Fig. 10. From Fig. 10, it can be seen that with the increase in the initial adsorbate concentration from 10 to 70 mg/L the removal efficiency of ICBSC decreased from 97.7 to 70.14% and from 99.20 to 75.03% for nitrate and phosphate, respectively, while the adsorption capacity increases from 17.09 to 85.9 mg/g and from 17.3 to 91.91 mg/g for nitrate and phosphate, respectively. Initially, the removal efficiency was very high for both adsorbates; it is because a large number of active sites were available for a low initial concentration of adsorbate, but with the increase in the concentration of adsorbate the active sites became insufficient for adsorption of the initial high concentration of adsorbate [22] resulting in poor removal efficiency. In contrast to removal efficiency, the adsorption capacity increases

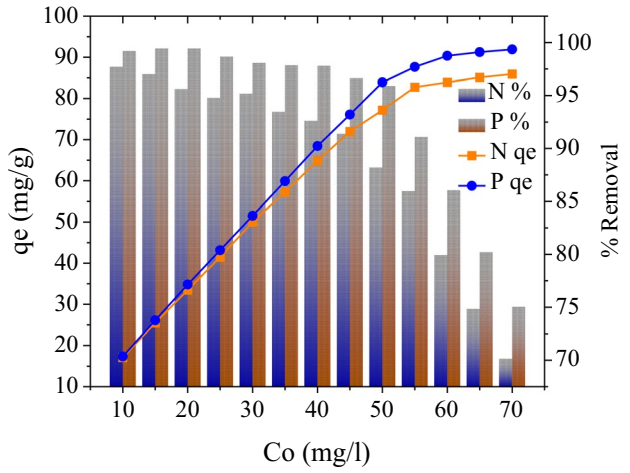

Fig. 10 Effect of initial concentration on q_e and % removal of ICSBC for nitrate and phosphate

with the increased adsorbate (nitrate and phosphate) initial concentration; this is because with the increase in the adsorbate initial concentration the adsorbate load increases over the ICSBC resulting in a high concentration gradient of adsorbate between the adsorbent surface and bulk of solution. During the adsorption phenomenon, the adsorbent continues to adsorb until it reaches its saturation point and 70 mL of 50 mg/L solution of adsorbate (nitrate or phosphate) was found to be the saturation point concentration for 0.04 g of ICSBC [15].

3.7 Adsorption isotherm study

To design an adsorption system for the adsorption of phosphate and nitrate on ICSBC, different adsorption isotherm models were applied to adsorption isotherm data. Adsorption isotherm models give a relation between the amount of adsorbate adsorbed on the adsorbent and the amount of adsorbate that remains in the bulk of the solution after equilibrium has been established. Freundlich, Langmuir, and Sips adsorption isotherm models were applied to experimental adsorption isotherm data; further details of these models are given below.

3.7.1 Freundlich adsorption isotherm model

In 1906, Freundlich put forward a model for explanation of the adsorption process which was then known as the Freundlich adsorption isotherm model [14, 29]. According to the Freundlich adsorption isotherm model, the adsorption energy of adsorbate ions is unequal and the surface of the adsorbent is heterogeneous on which multilayer adsorption occurs. The exponential decrease in the adsorption enthalpy with the rise in the adsorbate concentration is also suggested by this model [30]. In short, Freundlich has assumed in his model that the adsorption of adsorbate in adsorbent is physical. Freundlich models non-linear and linear are represented by Eqs. (9) and (10), respectively [15, 31].

$$q_e = K_f C_e^{\frac{1}{n}} \tag{9}$$

$$\log q_e = \log K_f + \frac{1}{n} \log C_e \tag{10}$$

$1/n$ and K_f are adsorption intensity and Freundlich constant relating to adsorption capacity, respectively, while C_e and q_e are the equilibrium concentration and adsorption capacity. The favorability adsorption process can be determined from the value of n [17, 31]. For the non-linear fitting of the Freundlich adsorption model to adsorption isotherm data of nitrate as well as phosphate adsorption on ICSBC, their respective equilibrium concentrations were plotted against adsorption capacities. The non-linear fitting plot of the Freundlich model for experimental data of nitrate and phosphate adsorption on ICSBC is shown in Figs. 11 and 12, respectively.

The values of Freundlich model parameters and R^2 are listed in Table 1 for nitrate and phosphate. The favorability of the adsorption process can be determined from the value of n. The value of n greater than 1 reveals that the adsorption process is chemical. In contrast, when the value of n is less than 1, it indicates that the adsorption process is physical and fits the Freundlich model [29]. From the values of R^2 ($N=0.90142$ and for $P=0.83852$) and from the fitting of the Freundlich curve to the data obtained from the adsorption of nitrate as well as phosphate on ICSBC (Figs. 11 and 12), it can be concluded that the Freundlich model does not fit well to experimental data. Along with the values of R^2 and fitting of the curve, the values of n ($N=0.2012$ and for $P=0.197$) and K_f ($N=50.2$ and for $P=59.03$) are also not in support of Freundlich model fitting to experimental data.

3.7.2 Langmuir adsorption isotherm model

In 1918, Irving Langmuir proposed the Langmuir adsorption isotherm model for the characterization of the adsorption process [14]. According to the Langmuir adsorption isotherm model, the adsorption energy of adsorbate adsorption on adsorbent is uniform, and the surface of adsorbent is homogeneous on which monolayer adsorption of adsorbate occurs which does not interact with each other. The nonlinear and linear forms of the Langmuir model can be represented by Eqs. (11) and (12), respectively [15, 25, 29].

$$q_e = \frac{q_{\max} K_L C_e}{1 + K_L C_e} \tag{11}$$

$$\frac{1}{q_e} = \frac{1}{K_L q_{\max} C_e} + \frac{1}{q_{\max}} \tag{12}$$

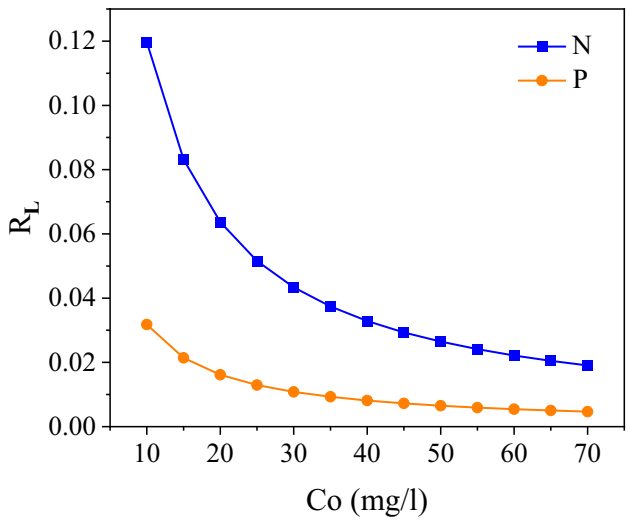

Fig. 11 Changes in the values of R_L for adsorption of nitrate and phosphate on ICSBC with the increase in concentration

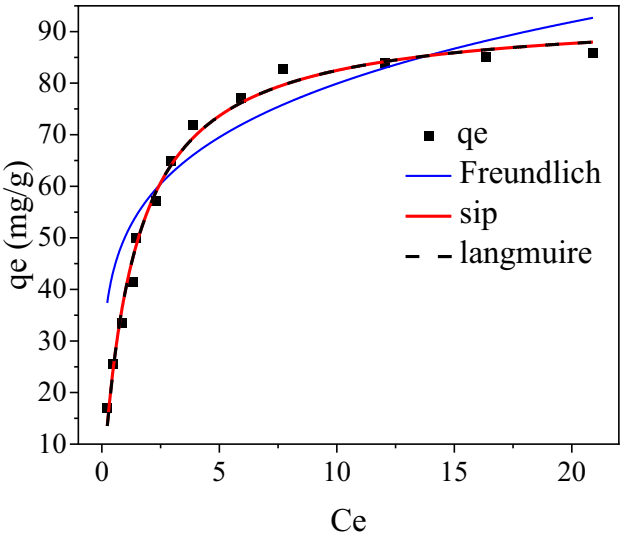

Fig. 12 Non-linear isotherm fitting for nitrate adsorption on ICSBC

K_L is the Langmuir constant and $q_{\max}$ is the maximum possible adsorption capacity of adsorbent (ICSBC) for adsorbate (nitrate or phosphate). The Langmuir fitting curve of the data obtained from the adsorption of nitrate as well as phosphate on ICSBC is shown in Figs. 12 and 13, respectively. The values of Langmuir parameters and R^2 are listed in Table 1.

Dimensionless separation factor (R_L) can also be used to check the applicability of the Langmuir model to obtained data. The values of R_L can be calculated using Eq. (13).

$$R_L = \frac{1}{1 + k_L C_o} \tag{13}$$

The R_L can have a value from 0 to > 1, but for a favorable adsorption process, the values of R_L should be $0 < R_L < 1$ [32]. For the process of adsorption of nitrate

Table 1 Isotherm adsorption model parameters for nitrate and phosphate adsorption on ICSBC

	Nitrate	Phosphate
Freundlich		
K_f (mg/g)	50.27676	59.03559
n	0.2012	0.19711
R^2	0.90142	0.83852
Langmuir		
q_m (mg/g)	93.68153	92.97788
K_L (L/mg)	0.73536	3.04488
R^2	0.98811	0.9637
Sips		
q_m (mg/g)	93.68153	89.92978
K	0.73536	4.16041
n	1	0.95796
R^2	1	0.96522

and phosphate over ICSBC, the values of R_L were found to be in the range from 0.119709 to 0.019057 and from 0.031798 to 0.00467, respectively, as shown in Fig. 11.

The values of R_L for nitrate as well as phosphate (Fig. 11) indicate that the process of adsorption of nitrate and phosphate on ICSBC is favorable. It can also be observed that with the increase in concentration, the value of R_L decreases which suggests that the increase in the concentration of adsorbate (nitrate and phosphate) adsorption process enhances. From the values of R^2 (N = 0.98811 and for P = 0.9637) and q_{max} (N = 93.68153 and for P = 92.97788) and from the fitting of the curve to the experimental data obtained from the adsorption of each adsorbate (nitrate and phosphate) on ICSBC, it can be concluded that the Langmuir adsorption isotherm model shows best fitting to obtained data.

3.7.3 Sips adsorption isotherm model

The Sips model amalgamates the Freundlich and Langmuir adsorption isotherm model, which describes the sorbent surface as homogeneous, and the adsorption of adsorbate is a cooperative process due to adsorbate-adsorbate interaction. It is explained in Eq. (14):

$$q_e = \frac{q_m \left(bC_e\right)^{\frac{1}{n}}}{1 + \left(bC_e\right)^{\frac{1}{n}}} \tag{14}$$

The fitting curve of the Sips adsorption isotherm model to isotherm data obtained from the adsorption of nitrate and phosphate on ICSBC is shown in Figs. 12 and 13, respectively. The values of Sips adsorption isotherm model parameters are listed in Table 1. From the fitting of the curve to obtained data and from the values of R^2 (N = 1 and for P = 0.965) and q_m (N = 93.6 and for P = 89.9), it can be concluded that the Sips adsorption isotherm model shows best fitting to experimental data from the adsorption of nitrate and phosphate over ICSBC [31].

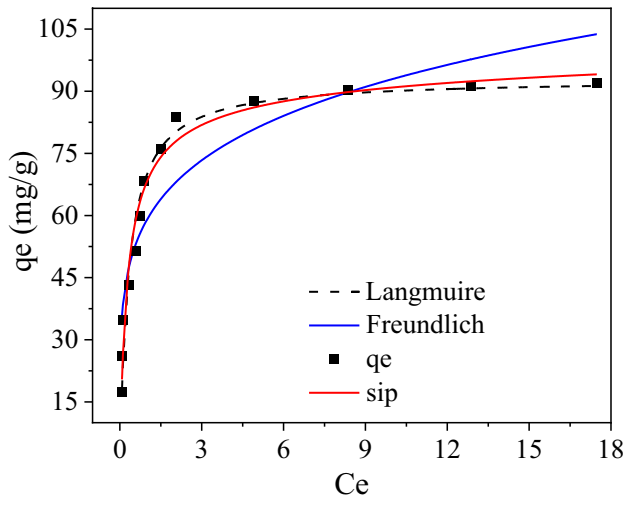

Fig. 13 Non-linear isotherm fitting for phosphate adsorption on ICSBC

From the values of different adsorption isotherm parameters and from the fitting of the curve to experimental data, it can be concluded that both Langmuir and Sips models show the best fitting to obtained data, which powerfully reveals the adsorption of nitrate and phosphate over ICSBC is chemical.

3.8 Effect of time on adsorption capacity and removal efficiency of nitrate and phosphate adsorption on ICSBC

Contact time has a significant effect on the adsorption process, and the time required for an adsorbent to attain equilibrium is mostly dependent on the nature of the adsorbent [14, 33]. In the case of biochar, the time required to attain equilibrium depends on the temperature at which the biochar is produced [34]. The effect of time was studied on the adsorption of nitrate and phosphate on ICSBC by changing the contact time from 5 to 420 min and keeping all other factors constant (pH = 2, adsorbent dose = 0.04 g, and Co = 50 mg/L). The result of contact time on the adsorption of nitrate and phosphate on ICSBC is shown in Fig. 14. From the figure, it can be seen that the removal efficiency and adsorption capacity of ICSBC for nitrate as well as phosphate increase with time. Initially, the rate of adsorption of nitrate and phosphate is very high because a large number of active sites were initially available on the surface of ICSBC, which resulted in fast adsorption of adsorbate on ICSBC. After some time (1 h), the rate of adsorption falls because most of the active sites were occupied by adsorbate (nitrate and phosphate) and a minimal number of active sites were available for adsorption of adsorbate which resulted in a slow rate of adsorbate adsorption on ICSBC [35]. A contact time of 180 min was considered to be the optimum contact (t_e) at which equilibrium is established between the adsorbate on the surface of the adsorbent and adsorbate in the bulk of the solution. After a contact time of 180 min, the study was extended up to 420 min but no significant increase was found in removal efficiency and adsorption capacity of ICSBC for nitrate and phosphate which suggests that a contact time of 180 min is an equilibrium contact time or optimum contact for adsorption of nitrate (% = 88.19, q_e = 77.17 mg/L) and phosphate (% = 83.91, q_e = 95.8 mg/g) on ICSBC.

3.9 Kinetic studies

The kinetic study is very helpful in investigating the dynamic interaction between adsorbate (nitrate and phosphate) and the surface of adsorbent (ICSBC). The kinetic study helps design a system for adsorption and the large-scale

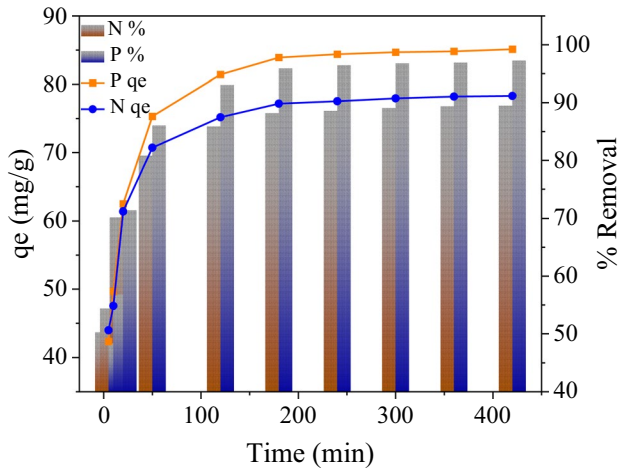

Fig. 14 Effect of contact time on q_e and % of ICSBC for nitrate and phosphate

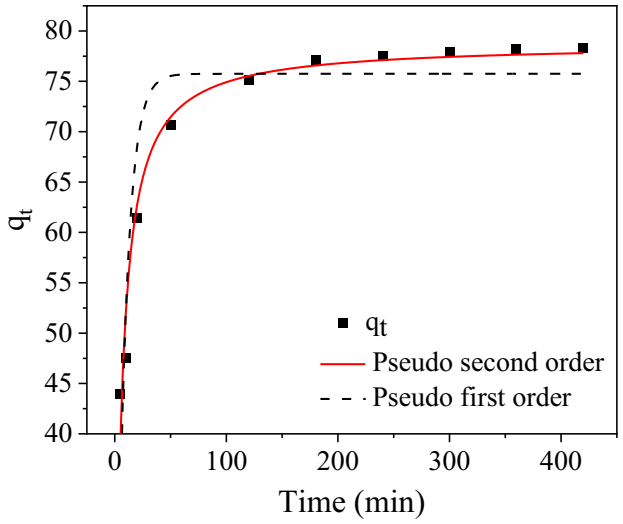

Fig. 15 Non-linear fitting of kinetic models for nitrate adsorption on ICSBC

application of adsorbents in wastewater treatment plants. For the kinetic study of nitrate and phosphate adsorption on ICSBC, pseudo-first and second-order kinetic models were applied to obtain kinetic data of nitrate and phosphate adsorption on ICSBC.

3.9.1 Pseudo-first-order kinetic model

Langergren in 1898 proposed a kinetic model known as a pseudo-first-order kinetic model [14]. The non-linear and linear form pseudo-first-order kinetic model is given by expressions (15) and (16), respectively [29].

$$q_t = q_e(1 - e^{K_1 t}) \tag{15}$$

$$\ln\left(q_e - q_t\right) = \ln\ q_e - K_1 t \tag{16}$$

t and K_1 are contact times and rate constants of the pseudo-first-order kinetic model, respectively. q_e and q_t are adsorption capacities at equilibrium and at any time t, respectively. The pseudo-first-order kinetic model was non-linearly applied to data obtained from the adsorption of nitrate and phosphate on ICSBC in the contact time effect study. For the fitting of the PFO kinetic model to obtain data, q_t was plotted against respective contact time t and the fitting of the PFO kinetic model to get data from the adsorption of nitrate and phosphate can be seen in Figs. 15 and 16, respectively. The PFO kinetic modal parameter values were calculated and listed in Table 2. From the value of R^2 (N = 0.83826 and for P = 0.88) and from the fitting of the curve to obtained data, it can be concluded that the PFO kinetic model does not fit well to the kinetic data of nitrate and phosphate adsorption onto ICSBC [31].

3.9.2 Pseudo-second-order kinetic model

Ho and McKay in 1999 proposed pseudo-second-order, also termed as Ho kinetic model. The non-linear and linear form of the pseudo-second-order kinetic model is given by expressions (17) and (18) [14, 29].

$$q_t = \frac{q_e^2 K_2 t}{1 + q_t K_2 t} \tag{17}$$

$$\frac{t}{q_t} = \frac{1}{K_2 q_e^2} + \frac{1}{q_e} t \tag{18}$$

$$h = k_2 q_e^2$$

The only thing new in this equation is K_2 and h which is a rate constant for the PSO kinetic model and initial adsorption rate, respectively [22, 36]. In the same way, as stated before, the PSO kinetic model was applied to kinetic data obtained from the adsorption of nitrate and phosphate on ICSBC. PSO kinetic model fitting plot for nitrate and phosphate can be seen in Figs. 15 and 16. The values of all PSO kinetic model parameters were calculated and listed in Table 2. As can be seen in Figs. 15 and 16, the PSO kinetic model curve shows best fitting to obtained kinetic data of nitrate and phosphate adsorption on ICSBC. An excellent value of R^2 (N = 0.9644 and for P = 0.9812) was obtained for both data, revealing that the PSO kinetic model is compatible with the received data. From the values of R^2 and the fitting of a curve to data, it can be concluded that the PSO kinetic model best fits experimental data of nitrate and phosphate adsorption on ICSBC [22].

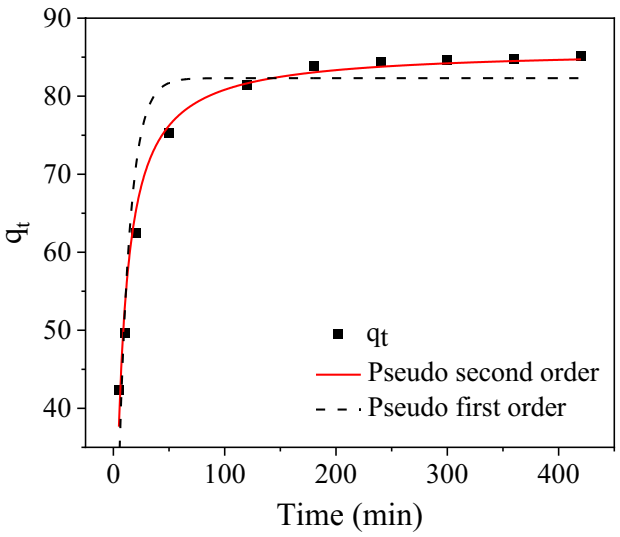

Fig. 16 Non-linear fitting of kinetic models for phosphate adsorption on ICSBC

Table 2 Isotherm kinetic models' parameter for nitrate and phosphate adsorption on ICSBC

	Nitrate	Phosphate
Pseudo-first-order kinetic model		
q_m (mg/g)	75.74661	82.31331
K_1	0.11715	0.098
R_2	0.83826	0.88009
Pseudo-second-order kinetic model		
q_m (mg/g)	78.74671	86.01302
K_2	0.00248	0.00181
R_2	0.96441	0.98122

By investigating the values in Table 2, it can be concluded that the PSO kinetic model is best fitting to the data obtained from the adsorption of nitrate and phosphate on ICSBC. From the assumption of the PSO kinetic model, it can be concluded the chemical phenomenon controls the rate of adsorption of nitrate and phosphate on ICSBC. From the adsorption isotherm studies and from the kinetic studies, it can be concluded that the adsorption of nitrate and phosphate on ICSBC is chemical [37, 38]. Table 3 summarizes the comparison of various adsorbents on the adsorption of nitrate and phosphate.

3.10 Desorption study or ICSBC regeneration experiment

It is economically desirable to regenerate and reuse the adsorbent (ICSBC) for the adsorptive removal of pollutants from wastewater [15]. In the case of phosphate and nitrate, the recovered phosphate and nitrate by desorption can be used as fertilizer, which further makes the regeneration of adsorbent desirable [44]. The remarkable decrease in the phosphate as well as nitrate adsorption efficiency on ICSBC with the increase in pH reveals the possibility of adsorbent (ICSBC) regeneration by desorption of adsorbate (nitrate and phosphate) from spent adsorbent (ICSBC) in alkaline solution [16]. Batch desorption experiments for both analytes were conducted using conditions as were applied to batch adsorption experiments, using 70 mL/0.2 M NaOH solution. The amount of analyte (nitrate or phosphate) released into the solution per gram of ICSBC is known as the desorption percentage. The desorption percentage is obtained when the q_e of desorption to q_e of adsorption is multiplied by 100. The q_e of desorption can be obtained using Eq. (18).

$$q_e = V\left(\frac{C_f}{M}\right) \quad (18)$$

where C_f is the concentration (mg/L) of analyte (nitrate or phosphate) after desorption from spent adsorbent (ICSBC), V is the volume (L) of alkaline solution used for desorption, and M is the mass (g) of spent ICSBC [15]. In the first cycle of desorption, a desorption percentage of 91.17% and 92.57% was obtained for nitrate and phosphate, respectively (Table 4). Four cycles of adsorption and desorption were carried out to check for how long the adsorbent (ICSBC) can be reused [23]. In the fourth cycle of adsorbent (ICSBC) reuse, the adsorptive removal efficiency of 70.11% and

Table 3 Comparative analysis of the nitrate and phosphate adsorption using different agricultural wastes as adsorbents

Adsorbents	N removal rate in %	P removal rate in %	q_e of N (mg g^{-1})	q_e of P (mg g^{-1})	Dosage (g L^{-1})	Initial conccentraion (mg L^{-1})	Ref.
Corn stalks	82.4	96.03	24.20	20.04	4	50	[39]
Corn stalks			13.61	22.88	2	100	[40]
Wheat straw			52.8	45.07	2	500	[41]
Biochar-MgAl LDH			28.26	73.69	2.5	10–50	[42]
SWR			0.06	0.96	20	5 and 19	[43]
ICSBC	88.19	95.89	77.17	83.93	4	50	Current studies

75.40% was obtained for nitrate and phosphate, respectively, which is quite excellent. These results indicate that ICSBC can be regenerated once used and has good potential to be reused again and again for adsorptive removal of nitrate and phosphate from wastewater.

3.11 Proposed mechanism of the nitrate and phosphate adsorption

The possible mechanism for the adsorption of nitrate and phosphate on ICSBC could be proposed on the information obtained in the current study. The mechanism of nitrate and phosphate adsorption can be explained by chemical and physical adsorption. From the kinetic and isotherm study, it is concluded that the nitrate and phosphate ions are chemically adsorbed on the surface of ICSBC. The possible mechanisms for the adsorption of nitrate and phosphate on the surface of ICSBC are as follows: (1) ligand exchange mechanism, (2) complexation, and (3) electrostatic attraction.

Ligand exchange mechanism is based on the exchange of nitrate and phosphate ions with the Fe hydroxyl present on the surface of Fe oxides. The FTIR analysis of ICSBC before and after the adsorption is presented in Fig. 5. The bands at 3440 cm^{-1} of ICSBC are attributed to the stretching vibration of –OH group, which belongs to the Fe hydroxyl on the Fe oxide surface. In the FTIR spectra of P-ICSBC, the band present at 1085 cm^{-1} corresponds to the presence P-O bond stretching vibration. Moreover, in the spectra of N-ICSBC, the peak at 1556 cm^{-1} corresponds to the N = O stretching vibration and NO_3 symmetric and asymmetric peaks are observed at 1384 cm^{-1} and 825 cm^{-1}. From Fig. 5, we can observed that in the spectra of P-ICSBC and N-ICSBC the –OH peaks disappear, while the peaks of P-O and N-O strengthen after the P and N adsorption. This indicate the exchange of ligand through the adsorption that results in replacing the hydroxyl groups by nitrate and phosphate ions. From the spectra, we can observed that the Fe peaks weaken after the adsorption of nitrate and phosphate that confirmed that iron coating plays a crucial role in the nitrate and phosphate adsorption process [45, 46].

Table 4 The efficiency of nitrate and phosphate desorption from ICSBC using NaOH solution

Cycle	Adsorption (%)		Desorption (%)	
	Nitrate	Phosphate	Nitrate	Phosphate
1	88.19	95.89	91.17	92.57
2	78.73	85.98	89.68	89.96
3	75.03	79.88	87.52	88.88
4	70.11	75.40	86.21	86.37

Electrostatic mechanism is based on the electrostatic interaction between the negatively charged nitrate and phosphate ions and positively charged surface functional group on ICSBC. Electrostatic interaction plays an important role in the removal of negatively charged nitrate and phosphate ions which is verified by the increase in the adsorption capacity with the decrease in the pH (Fig. 9). The higher adsorption capacity of nitrate and phosphate ions can be attributed to the attractive electrostatic interaction between negatively charged ions and positively charged surface of biochar (ICSBC) at a pH value lower than pH_{PZC} (pH_{PZC} = 5). At $pH < pH_{PZC}$, the surface of the adsorbent (ICSBC) is positively charged due to the protonation of oxygen-based functional groups and will electrostatically attract negatively charged nitrate and phosphate ions and result in higher adsorption capacity. At $pH > pH_{PZC}$, the surface of the adsorbent (ICSBC) is negatively charged due to deprotonation of oxygen-based functional groups and will electrostatically repel negatively charged nitrate and phosphate ions resulting in lower adsorption capacity. With the increase in the pyrolysis temperature, the extent of carbonization enhanced resulting in higher electrostatic interaction between the surface of biochar and metal ions [47].

The complexation mechanism is based on the formation of a coordination complex between the nitrate and phosphate ions and surface functional groups. This mechanism is more predominant in the biochar prepared at low temperature due to a large number of oxygen-based functional groups on the surface of biochar prepared at low temperature as compared to biochar prepared at high temperature. In short, biochar prepared from agricultural waste shows high complexation and ion exchange potential for the adsorption of adsorbate. The complexation of nitrate and phosphate ions with the surface functional groups has been considered as a significant mechanism for the adsorptive removal of nitrate and phosphate ions which is further verified by kinetic and isotherm study which also suggest that adsorption of nitrate and phosphate ions onto ICSBC is chemisorption involving sharing and exchange of electron. The complexation mechanism is also verified from the FTIR spectrum of N-ICSBC and P-ICSBC (Fig. 5). In the FTIR spectrum, the peaks for O–H, C=O, Fe–O, C–O–C, and C=C groups can be observed. These oxygen-based functional groups can easily form complexes with the nitrate and phosphate ions resulting in the chemisorption of nitrate and phosphate ions on the surface of ICSBC [47].

$$R - OH + NO_3^- \rightarrow R - OH \cdots NO_3^-$$

$$Fe - OH + NO_3^- \rightarrow Fe - OH \cdots NO_3^-$$

$$R - C = O + NO_3^- \rightarrow R - C = O \cdots NO_3^-$$

Table 5 Cost analysis of various commercially available adsorbents and ICSBC

Adsorbent	Cost ($/g)	Reference
Mesoporous silica	0.068	[48]
Nanozeolite	0.0300	[49]
Copper impregnated tufa	0.0066	[50]
Chitosan-calcite	0.2646	[51]
Titania/graphene oxide	0.1875	[52]
ICSBC	0.0038	Current studies

$$R - OH + PO_4^- \rightarrow R - OH \cdots PO_4^-$$

$$Fe - OH + PO_4^- \rightarrow Fe - OH \cdots PO_4^-$$

$$R - C = O + PO_4^- \rightarrow R - C = O \cdots PO_4^-$$

3.12 Cost analysis

Commercially available adsorbents for large-scale applications are hampered due to their high operational cost, difficulty in regeneration, and relatively high prices. Therefore, it is necessary to introduce adsorbents that are low-cost, renewable, and locally available materials for the treatment of wastewater. If the adsorbents are readily available and low-cost, it provides a feasible treatment for the adsorption process. To compare different materials, adsorbent cost is an important parameter. Table 5 shows the cost of our prepared adsorbent and compares it with commercially available adsorbents. The cost of the adsorbents depends upon numerous factors like their sources (agricultural/domestic/industrial/natural/by-product or synthesized product), recycling, treatment conditions, and durability.

4 Conclusion

Biochar derived from *P. hysterophorus* emerges as a promising biosorbent class for removing nitrate and phosphate from municipal and industrial water sources. This work prepared biochar from the *P. hysterophorus* stem to remove nitrate and phosphate from water. The prepared biochar was then impregnated with $FeCl_3$ and $FeSO_4$ to enhance its efficiency. Batch sorption experiments were conducted to examine the optimum adsorption conditions. The investigations revealed that optimum pH of 2, contact time 180 min, the adsorbent dosage of 0.04 g, and the adsorbate initial concentration of 50 mg/L are the ideal parameters for the adsorptive removal of nitrate and phosphate. The maximum removal efficacy for nitrate and phosphate was 88.19% and 95.89%. Likewise, the optimum adsorption capacity for nitrate and phosphate was 77.17 mg/g and 83.93 mg/g. To examine the surface functional group, FTIR analysis was carried out. SEM and EDS analysis were carried out for surface morphology and elemental analysis. Freundlich, Langmuir, and Sips isotherm models were used to assess equilibrium models. Among them, the Langmuir isotherm model best fits the experimental data with an R^2 value of 0.9811 for nitrate and 0.963 for phosphate, respectively, indicating that adsorption occurs via chemisorption. PFO and PSO are used to study the kinetic models. Among them, the PSO kinetic model shows good fitting with an R^2 value of 0.9644 for nitrate and 0.98122 for phosphate. From this discussion, we concluded that ICSBC is practically applicable for removing nitrate and phosphate from water. In short, this method of impregnated biochar presents new prospects for finding economical and efficient treatments for removing nitrate, phosphate, and other pollutants from water using waste materials.

Author contribution **Izaz ul Islam**: Writing the original draft, experimentation, discussing the results, commenting on the manuscript, critical feedback, organization, helped shape the research, design of the article and corrections. **Mushtaq Ahmad:** Writing the original draft, experimentation, discussing the results, commenting on the manuscript, critical feedback, organization, and helped shape the research, design of the article and corrections. **Behzad Shah**: Carried out the characterization. **Hafiz Muhammad Ahmad**: Helped in manuscript revision, graphical work, and data analysis. **Sara Janiad**: Helped in the manuscript revision and data analysis. **Nasrullah Shah**: Discussed the results and commented on the manuscript. **Erdal Yabalak**: Writing and correcting the original draft, review and editing, discussed the results, commented on the manuscript, critical feedback, and organization, and helped shape the research, design of the article, corrections and supervision. All authors have read and agreed to the published version of the manuscript.

Funding Open access funding provided by the Scientific and Technological Research Council of Türkiye (TÜBİTAK).

Data availability All data generated or analyzed during this study are included in this published article [and its supplementary information files].

Declarations

Ethical approval Not applicable.

Competing interests The authors declare no competing interests.

Open Access This article is licensed under a Creative Commons Attribution 4.0 International License, which permits use, sharing, adaptation, distribution and reproduction in any medium or format, as long as you give appropriate credit to the original author(s) and the source, provide a link to the Creative Commons licence, and indicate if changes were made. The images or other third party material in this article are included in the article's Creative Commons licence, unless indicated otherwise in a credit line to the material. If material is not included in the article's Creative Commons licence and your intended use is not permitted by statutory regulation or exceeds the permitted use, you will need to obtain permission directly from the copyright holder. To view a copy of this licence, visit http://creativecommons.org/licenses/by/4.0/.

References

1. Zhang M et al (2020) Evaluating biochar and its modifications for the removal of ammonium, nitrate, and phosphate in water. Water Res 186:116303
2. Karthikeyan P, Meenakshi S (2021) Development of sodium alginate@ ZnFe-LDHs functionalized beads: Adsorption properties and mechanistic behaviour of phosphate and nitrate ions from the aqueous environment. Environ Chem Ecotoxicol 3:42–50
3. Eltaweil AS et al (2021) Chitosan based adsorbents for the removal of phosphate and nitrate: a critical review. Carbohydr Polym 274:118671
4. Priya E, Kumar S, Verma C, Sarkar S, Maji PK (2022) A comprehensive review on technological advances of adsorption for removing nitrate and phosphate from waste water. J Water Process Eng 49:103159
5. Al-Hazmi HE, Lu X, Grubba D, Majtacz J, Badawi M, Mąkinia J (2023) Sustainable nitrogen removal in anammox-mediated systems: microbial metabolic pathways, operational conditions and mathematical modelling. Sci Total Environ 868:161633
6. Prashantha Kumar TKM, Mandlimath TR, Sangeetha P, Revathi SK, Ashok Kumar SK (2016) Selective removal of nitrate and phosphate from wastewater using nanoscale materials. Nanosci Food Agric 3:199–223
7. Manjunath SV, Kumar M (2018) Evaluation of single-component and multi-component adsorption of metronidazole, phosphate and nitrate on activated carbon from Prosopıs julıflora. Chem Eng J 346:525–534
8. Banu HAT, Karthikeyan P, Vigneshwaran S, Meenakshi S (2020) Adsorptive performance of lanthanum encapsulated biopolymer chitosan-kaolin clay hybrid composite for the recovery of nitrate and phosphate from water. Int J Biol Macromol 154:188–197
9. Ahmed MJ, Hameed BH, Hummadi EH (2020) Review on recent progress in chitosan/chitin-carbonaceous material composites for the adsorption of water pollutants. Carbohydr Polym 247:116690
10. Huang X, Liao X, Shi B (2009) Adsorption removal of phosphate in industrial wastewater by using metal-loaded skin split waste. J Hazard Mater 166:2–3
11. Yakout SM, Salem NA, Mostafa AA, Abdeltawab AA (2019) Relation between biochar physicochemical characteristics on the adsorption of fluoride, nitrite, and nitrate anions from aqueous solution. Part Sci Technol 37(1):118–122
12. Bashar HMK et al (2021) A mytstic weed, Parthenium hysterophorus: threats, potentials and management. Agronomy 18(11):1514. https://doi.org/10.3390/agronomy11081514
13. Singh RK, Kumar S, Kumar S, Kumar A (2008) Development of parthenium based activated carbon and its utilization for adsorptive removal of p-cresol from aqueous solution. J Hazard Mater 155(3):523–535
14. Ahmad M, Islam IU, Ahmad M, Shah, Ihsan R (2022) Preparation of iron modified biochar from rice straw and its application for the removal of lead (pb + 2) from lead contaminated water by adsorption. Chem Pap. https://doi.org/10.1007/s11696-022-02118-y
15. Fetene Y, Addis T (2020) Adsorptive removal of phosphate from wastewater using Ethiopian rift pumice: batch experiment. https://doi.org/10.1177/1178622120969658
16. Lalley J, Han C, Li X, Dionysiou DD, Nadagouda MN (2016) Phosphate adsorption using modified iron oxide-based sorbents in lake water: kinetics, equilibrium, and column tests. Chem Eng J 284:1386–1396. https://doi.org/10.1016/j.cej.2015.08.114
17. Hoang LP et al (2019) Removal of Cr(Vi) from aqueous solution using magnetic modified biochar derived from raw corncob. New J Chem 43(47):18663–18672
18. Bardalai M, Mahanta DK (2018) ScienceDirect Characterisation of Biochar produced by pyrolysis from Areca Catechu Dust. Mater Today Proc 5(1):2089–2097. https://doi.org/10.1016/j.matpr.2017.09.205
19. Yahya MD, Obayomi KS, Abdulkadir MB, Iyaka YA, Olugbenga AG (2020) Characterization of cobalt ferrite-supported activated carbon for removal of chromium and lead ions from tannery wastewater via adsorption equilibrium. Water Sci Eng. https://doi.org/10.1016/j.wse.2020.09.007
20. Chandra S, Bhattacharya J (2019) Influence of temperature and duration of pyrolysis on the property heterogeneity of rice straw biochar and optimization of pyrolysis conditions for its application in soils. J Clean Prod 215:1123–1139
21. Rivera KKP et al (2017) Hexavalent chromium removal from aqueous solution by adsorbents synthesized from groundwater treatment residuals sustainable Environment Research Hexavalent chromium removal from aqueous solution by adsorbents synthesized from groundwater treatment residu. No July. https://doi.org/10.1016/j.serj.2017.04.001
22. Waktole Y, Seid B, Mereta T, Fufa F (2019) Simultaneous removal of nitrate and phosphate from wastewater using solid waste from factory. Appl Water Sci 9(2):1–10. https://doi.org/10.1007/s13201-019-0906-z
23. Ali H, Banu T, Karthikeyan P, Meenakshi S (2021) Removal of nitrate and phosphate ions from aqueous solution using zirconium encapsulated Chitosan quaternized beads: Preparation, characterization and mechanistic performance. Results Surf Interfaces 3:100010. https://doi.org/10.1016/j.rsurfi.2021.100010
24. Mahdavi S, Akhzari D (2016) The removal of phosphate from aqueous solutions using two nano-structures: copper oxide and carbon tubes. Clean Technol Environ Policy 18(3):817–827. https://doi.org/10.1007/s10098-015-1058-y
25. Katal R, Sharifzadeh M, Taher H, Esfandian H (2012) Journal of Industrial and Engineering Chemistry Kinetic, isotherm and thermodynamic study of nitrate adsorption from aqueous solution using modified rice husk. J Ind Eng Chem 18(1):295–302. https://doi.org/10.1016/j.jiec.2011.11.035
26. Zhang Q et al (2015) Highly efficient phosphate sequestration in aqueous solutions using nanomagnesium hydroxide modified polystyrene materials. Ind Eng Chem Res 54(11):2940–2949. https://doi.org/10.1021/ie503943z
27. Lu J, Liu D, Hao J, Zhang G, Lu B (2015) Phosphate removal from aqueous solutions by a nano-structured Fe-Ti bimetal oxide sorbent. Chem Eng Res Des 93:652–661. https://doi.org/10.1016/j.cherd.2014.05.001
28. Paquin F, Rivnay J, Salleo A, Stingelin N, Silva C (2015) Engineered graphene-nanoparticle aerogel composites for efficient removal of phosphate from water. J Mater Chem C 3:10715–10722. https://doi.org/10.1039/b000000x
29. Akalin HA, Hiçsönmez Ü, Yilmaz H (2018) Removal of cesium from aqueous solution by adsorption onto Sivas-Yildizeli (Türkiye) vermiculite: equilibrium, kinetic and thermodynamic studies. J Turkish Chem Soc Sect A: Chem 5(1):85–116
30. Liu C, Liang X, Liu J, Lei X, Zhao X (2017) Preparation of the porphyrin-functionalized cotton fiber for the chromogenic detection and efficient adsorption of Cd2 + ions. J Colloid Interface Sci 488:294–302
31. Islam IU, Ahmad M, Ahmad M, Rukh S, Ullah I (2022) Kinetic studies and adsorptive removal of chromium cr(VI) from contaminated water using green adsorbent prepared from agricultural waste, rice straw. Eur J Chem 13(1):78–90. https://doi.org/10.5155/eurjchem.13.1.78
32. Parthasarathy P, Narayanan SK (2014) Adsorption of lead(II) ions from simulated wastewater using natural waste: a kinetic, thermodynamic and equilibrium study P. Environ Prog Sustain Energy 33(3):676–680

33. Malik H, Qureshi UA, Muqeet M, Mahar RB, Ahmed F, Khatri Z (2018) Removal of lead from aqueous solution using polyacrylonitrile/magnetite nanofibers. Environ Sci Pollut Res 25(4):3557–3564
34. Shen Z et al (2019) Effect of production temperature on lead removal mechanisms by rice straw biochars. Sci Total Environ 655:751–758
35. Zhou X, Liu Y, Zhou J, Guo J, Ren J, Zhou F (2018) Efficient removal of lead from aqueous solution by urea-functionalized magnetic biochar: Preparation, characterization and mechanism study. J Taiwan Inst Chem Eng 91:457–467
36. Haloi N, Sarma HP, Chakravarty P (2013) Biosorption of lead (II) from water using heartwood charcoal of Areca catechu: equilibrium and kinetics studies. Appl Water Sci 3(3):559–565
37. Di Chen Y, Ho SH, Wang D, su Wei Z, Chang JS, Ren N (2017) Lead removal by a magnetic biochar derived from persulfate-ZVI treated sludge together with one-pot pyrolysis. Bioresour Technol 247(July):463–470, 2018
38. Xu P, Ming G, Lian D, Yan M, Chen M, Lai C (2016) Fabrication of reduced glutathione functionalized iron oxide nanoparticles for magnetic removal of pb (II) from wastewater. J Taiwan Inst Chem Eng 0:1–9. https://doi.org/10.1016/j.jtice.2016.11.031
39. Wang L et al (2018) Comparative analysis on adsorption properties and mechanisms of nitrate and phosphate by modified corn stalks. RSC Adv 8(64):36468–36476. https://doi.org/10.1039/C8RA06617E
40. Fan C, Zhang Y (2018) Adsorption isotherms, kinetics and thermodynamics of nitrate and phosphate in binary systems on a novel adsorbent derived from corn stalks. J Geochem Explor 188:95–100. https://doi.org/10.1016/j.gexplo.2018.01.020
41. Xu X, Gao B-Y, Yue Q-Y, Zhong Q-Q (2010) Preparation of agricultural by-product based anion exchanger and its utilization for nitrate and phosphate removal. Bioresour Technol 101(22):8558–8564. https://doi.org/10.1016/j.biortech.2010.06.060
42. Alagha O, Manzar MS, Zubair M, Anil I, Mu'azu ND, Qureshi A (2020) Comparative adsorptive removal of phosphate and nitrate from wastewater using biochar-MgAl LDH nanocomposites: coexisting anions effect and mechanistic studies. Nanomaterials 10(2). https://doi.org/10.3390/nano10020336
43. Berkessa YW, Mereta ST, Feyisa FF (2019) Simultaneous removal of nitrate and phosphate from wastewater using solid waste from factory. Appl Water Sci 9(2):28. https://doi.org/10.1007/s13201-019-0906-z
44. Xie J, Wang Z, Fang D, Li C, Wu D (2014) Green synthesis of a novel hybrid sorbent of zeolite/lanthanum hydroxide and its application in the removal and recovery of phosphate from water. J Colloid Interface Sci 423:13–19. https://doi.org/10.1016/j.jcis.2014.02.020
45. Bishayee B, Chatterjee RP, Ruj B, Chakrabortty S, Nayak J (2022) Strategic management of nitrate pollution from contaminated water using viable adsorbents: an economic assessment-based review with possible policy suggestions. J Environ Manage 303:114081. https://doi.org/10.1016/j.jenvman.2021.114081
46. Qin Y et al (2023) Phosphate removal mechanisms in aqueous solutions by three different Fe-modified biochars. Int J Environ Res Public Health 20(1). https://doi.org/10.3390/ijerph20010326
47. Abbas Z et al (2018) A critical review of mechanisms involved in the adsorption of organic and inorganic contaminants through biochar. Arab J Geosci 11(16):448. https://doi.org/10.1007/s12517-018-3790-1
48. Sarafraz H, Alahyarizadeh G, Minuchehr A, Modaberi H, Naserbegi A (2019) Economic and efficient phosphonic functional groups mesoporous silica for uranium selective adsorption from aqueous solutions. Sci Rep 9(1):9686. https://doi.org/10.1038/s41598-019-46090-2
49. Pham T-H, Lee B-K, Kim J (2016) Improved adsorption properties of a nano zeolite adsorbent toward toxic nitrophenols. Process Saf Environ Prot 104:314–322. https://doi.org/10.1016/j.psep.2016.08.018
50. Bajić ZJ et al (2016) Adsorption study of arsenic removal by novel hybrid copper impregnated tufa adsorbents in a batch system. Clean (Weinh) 44(11):1477–1488. https://doi.org/10.1002/clen.201500765
51. Pap S et al (2020) Low-cost chitosan-calcite adsorbent development for potential phosphate removal and recovery from wastewater effluent. Water Res 173:115573. https://doi.org/10.1016/j.watres.2020.115573
52. Fu C-C, Juang R-S, Huq MM, Hsieh C-T (2016) Enhanced adsorption and photodegradation of phenol in aqueous suspensions of titania/graphene oxide composite catalysts. J Taiwan Inst Chem Eng 67:338–345. https://doi.org/10.1016/j.jtice.2016.07.043

Publisher's Note Springer Nature remains neutral with regard to jurisdictional claims in published maps and institutional affiliations.